International Journal for Multidisciplinary Research (IJFMR)
E-ISSN: 2582-2160 ● Website: www.ijfmr.com ● Email: editor@ijfmr.com

# Numerical Investigation of Hypersonic Flow Over a Rectangular Cavity at Mach 6.3

**Bhoomika Venugopal[1], Jayahar Sivasubramanian[2]**

[1,2]Department of Aerospace and Automotive Engineering, M. S. Ramaiah University of Applied Sciences, Bangalore

**Abstract**

This study investigates hypersonic flow over a rectangular cavity, focusing on the influence of cavity aspect ratio (L/D), Reynolds number and thermochemical non-equilibrium flows. Cavities, such as those in landing gear bays or weapon compartments, can produce intense local heating, strong acoustic waves, and large pressure variations. The cavity aspect ratio affects the shear-layer shape, the extent of recirculation zones, and the operating regime of the cavity. Reynolds number governs the boundary-layer growth, separation, further shaping the flow field. Simulations were conducted using the open-source SU2 CFD solver with compressible, viscous flow models for different cavity aspect ratios and Reynolds numbers. The results highlight how these parameters alter flow structures, pressure distribution, and aerodynamic heating inside and around the cavity. Non-equilibrium effects, particularly vibrational excitation and dissociation, were found to modify temperature fields and reduce peak heating compared to equilibrium predictions. The findings provide useful guidance for designing thermal protection systems and implementing flow control strategies in hypersonic vehicles.

**Keywords:** Hypersonic flow, Rectangular Cavity, Aspect Ratio, Aerodynamic Heating.

## 1. Introduction

Cavities are openings or hollow areas on the exterior of aerospace vehicles that are used for vital practical functions including housing sensor ports, armament bays, air intakes, exhausts, or landing gear compartments. As they enable internal system storage and deployment while preserving aerodynamic efficiency and stealth, these cavities are essential to mission design and performance, particularly in military and high-speed vehicles.

When a hypersonic freestream flows over a cavity, a thin shear layer forms across its opening, trapping the recirculating flow inside. This trapped flow interacts with shock waves and creates unsteady oscillations. The cavity's aspect ratio (L/D) determines whether the flow behaves in an open, transitional, or closed manner, while the Reynolds number affects how the boundary layer grows, separates, and transitions to turbulence. Understanding these dependencies is crucial for predicting aerodynamic loads and heating patterns.

## 2. Literature Review

Several studies have addressed the complex aerodynamics of cavities in high-speed flows. Hahn [1] carried out wind tunnel experiments on hypersonic cavities, capturing details of shear-layer oscillations and the resulting pressure changes across different shapes. Nestler [2] looked at how shock waves interact

with shear layers at high Mach numbers, showing that these interactions can significantly increase unsteady surface pressures. Morgenstern [3] used both experiments and simulations to investigate cavity flow regimes and acoustic resonance under supersonic and hypersonic conditions. Jackson [4] focused on how the length-to-depth ratio affects recirculation zones and heat distribution within the cavity.

While these works have expanded our knowledge of cavity flow behaviour, there is still limited research that systematically examines a broad range of L/D ratios and Reynolds numbers at hypersonic speeds. Experimental and numerical investigations into cavity flows have laid an essential foundation for understanding the complex aerodynamics that emerge when high-speed flow passes over recessed geometries.

Additional studies have provided further insights into the underlying physics. Everhart [5] examined the role of upstream pressure gradients on cavity heating, demonstrating how these gradients can significantly change local heat-flux levels. Wahba [6] performed numerical and analytical work on steady rectangular cavity flows at high Reynolds numbers, offering valuable scaling relationships for mean flow features. Thomas [7] investigated 3D modeling in design and analysis of hypersonic cavities, particularly when aero- thermodynamic loads (pressure and heat flux) are critical. Singh [8] contributed combined experimental and numerical datasets on open rectangular cavities that are particularly useful for validating computational models across different L/D values. More recent high-fidelity simulations, such as those by Redding [9], have incorporated thermochemical non-equilibrium and conjugate heat transfer, revealing that gas chemistry and material conduction can further complicate surface heating predictions at very high enthalpy conditions. D Passiatore [10] examined turbulence sustains vibrational non-equilibrium, with significant effects on wall heat flux and energy redistribution.

Although these works have clarified important mechanisms such as shear-layer instability, vortex impingement, shock shear-layer coupling, and recirculation dynamics comparisons across studies remain challenging. Differences in test conditions, the narrow range of L/D ratios and Reynolds numbers explored in most campaigns, and variations in diagnostic and numerical methods mean that a comprehensive, predictive framework for hypersonic cavity behaviour is still lacking. In particular, experimental datasets often covers only a limited parameter space due to facility constraints, while numerical studies tend to focus on a single flow regime or use specific turbulence and chemistry models that limit generalization. Furthermore, very few studies have examined the combined influence of L/D and Reynolds number under consistent hypersonic conditions.

The present work addresses these gaps by performing a systematic computational investigation of hypersonic flow over a rectangular cavity, varying the L/D ratio across regimes from open to closed, and sweeping Reynolds numbers to capture laminar transitions. This work also focuses on the thermochemical non-equilibrium flows using two temperature model and 5 species [9]. The study characterizes how shear-layer structure, recirculation patterns, pressure contours, and surface heat-flux distributions evolve with these parameters. By comparing simulation trends with key experimental observations from Hahn, Nestler, Jackson, and Singh, this work aims to evaluate model fidelity, highlight where additional measurements are most needed, and provide design-relevant guidance on how geometry and flow conditions affect peak heating and unsteady loads—critical factors for thermal protection and flow-control strategies in hypersonic vehicles.

## 3. Governing Equations

For hypersonic flow over a rectangular cavity, the governing equations are the compressible Navier–

Stokes equations and thermochemical non-equilibrium Navier-Stokes equations. These equations account for conservation of mass, momentum, and energy, and are essential for capturing key features such as shock waves, boundary layers, and recirculation zones that are characteristic of hypersonic cavity flows. When needed, thermochemical non-equilibrium models are incorporated for high-enthalpy flows, accounting for vibrational and chemical relaxation effects. For solving the effect of cavity aspect ratio and Reynolds number, the SU2 CFD solver uses the compressible Navier-Stokes equations [11]. It is expressed in the differential form as,

$$\mathcal{R}(U) = \frac{\partial U}{\partial t} + \nabla.\overline{\mathrm{F}}^{c}(U) - \nabla.\overline{F}^{v}(U, \nabla U) - S = 0 \qquad (1)$$

Where,

U: Vector of conserved variables (density, momentum components and total energy).

$$U = \{\rho, \rho\overline{v}, \rho E\}^{T} \qquad (2)$$

$\overline{\mathrm{F}}^{c}$(U): Convective (Inviscid) fluxes account for transport by the flow itself, including shock phenomena that are prominent in hypersonic regimes.

$$\overline{F}^{c} = \begin{Bmatrix} \rho\overline{v} \\ \rho\overline{v}\otimes\overline{v} + \overline{I}p \\ \rho E\overline{v} + p\overline{v} \end{Bmatrix} \qquad (3)$$

$\overline{F}^{v}(U, \nabla U)$: Viscous fluxes capture effects of viscosity and heat conduction, essential for proper modelling of boundary layers, shear layers, and recirculation inside/near the cavity.

$$\overline{F}^{v} = \begin{Bmatrix} \dot{\overline{\tau}} \\ \overline{\tau}.\overline{v} + \kappa\nabla T \end{Bmatrix} (4)$$

*S* is Source terms (can represent chemical reactions, external forces, or geometric effects), ρ is the fluid density, E is the total energy per unit mass, p is the static pressure, T is the temperature and $\kappa$ is the thermal conductivity.

Hypersonic cavity flows experience very strong gradients (shocks, boundary layers, separated flows, shear layers), which this general conservative formulation accurately captures especially essential in shock-capturing numerical schemes.

To simulate hypersonic flows in thermochemical non-equilibrium, SU2-NEMO solves the Navier-Stokes equations for reacting flows [11], expressed in differential form as,

$$\mathcal{R}(U) = \frac{\partial U}{\partial t} + \nabla.\overline{\mathrm{F}}^{c}(U) - \nabla.\overline{F}^{v}(U, \nabla U) - S = 0 \qquad (5)$$

Where,

$$U = \{\rho_1, \dots, \rho_{ns}, \rho\overline{v}, \rho E, \rho E_{ve}\}^{T} \qquad (6)$$

Convective fluxes and viscous fluxes are

$$\overline{\mathrm{F}}^{c} = \begin{Bmatrix} \rho_1\overline{v} \\ . \\ . \\ . \\ \rho_{ns}\overline{v} \\ \rho\overline{v}\otimes\overline{v} + \overline{I}p \\ \rho E\overline{v} + p\overline{v} \\ \rho E_{ve}\overline{v} \end{Bmatrix} \qquad (7)$$

$$\overline{F}^{v} = \begin{Bmatrix} -\bar{J}_1 \\ . \\ . \\ -\bar{J}_{ns} \\ \overline{\tau} \\ \overline{\tau}.\overline{v} + \sum_k \kappa k \nabla T_k - \sum_s J \bar{J}_s h_s \\ \kappa_{ve} \nabla T_{ve} - \sum_s \bar{J}_s E_{ve} \end{Bmatrix} \quad (8)$$

Thermochemical non-equilibrium occurs when the energy distribution among different molecular modes (translational, rotational, vibrational, and electronic) is not described by a single temperature. In hypersonic cavity flows, these effects are most pronounced in regions behind strong shocks and inside recirculation zones, where molecules experience sudden temperature jumps and finite-rate processes. The choice of species to be incorporated to model chemical non-equilibrium depends largely on the species [9]. The five species air model is used for non-equilibrium hypersonic flow simulations are N, O, $N_2$, $0_2$ and NO [9]. In the 5-species air model, the following key reactions are included:

- Dissociation/recombination of $N_2$ and $O_2$:
- $N_2 \leftrightarrow 2N$
- $O_2 \leftrightarrow 2O$
- Formation/decomposition of NO:
- $N+O_2 \leftrightarrow NO+O$
- $O+N_2 \leftrightarrow NO+N$
- $NO \leftrightarrow N+O$

Where, N: atomic nitrogen, O is atomic oxygen, $N_2$ is molecular nitrogen, $O_2$ is molecular oxygen and NO is nitric oxide.

The 5-species model captures the major chemical changes and energy exchanges occurring in the flow, allowing for realistic simulation of aerodynamic heating and surface reactions. In this study, two-temperature model and 5 species are employed.

## 4. Methods and Methodology

This work explores the behavior of hypersonic flow over a two-dimensional rectangular cavity using a comprehensive computational approach, with results benchmarked against established experimental data from the literature. The goal was to capture and understand the key flow phenomena such as shear layer interactions, recirculating regions inside the cavity, and the oscillations in pressure while systematically studying how these features change with variations in Reynolds number and cavity geometry.

### A. Computational Methodology

The numerical simulations were performed using the open-source SU2 CFD solver, which is well-suited for high-speed compressible flows as it solves the Navier–Stokes equations in a density-based framework. The geometry consisted of a flat plate with a rectangular cavity, tested at different aspect ratio (L/D) and Reynolds numbers to identify trends in flow structure and stability. The computational mesh was generated in Pointwise, using a structured grid layout with deliberate clustering near the cavity's leading and trailing edges. This refinement ensured accurate resolution of the shear layer formation, shock impingement zones, and steep gradients typical of hypersonic regimes. Mesh independence studies were carried out to confirm that the grid density was sufficient for capturing the essential flow features. The boundary conditions

replicated those of hypersonic wind tunnel experiments: a uniform freestream inflow, adiabatic no-slip walls along the plate and cavity surfaces, and a supersonic outflow at the downstream boundary.

### B. Validation with Experimental Data

To establish credibility in the computational setup, the simulation results were validated against the hypersonic cavity experiments of Morgenstern and Chokani (1994) [3]. Validation metrics included Mach number profiles at different x/D locations, velocity profiles at selected (x/D) locations, and surface heat transfer ratio of the cavity. Experimental uncertainty bounds were considered during the comparison, providing a realistic measure of agreement. The close match between numerical and experimental results confirmed the accuracy of the setup and justified extending the analysis to Reynolds numbers and geometries beyond the experimental database. Through a combination of precise mesh generation, robust numerical schemes, and thorough validation, this methodology offers a reliable framework for examining how geometric configuration and flow conditions influence hypersonic cavity flow behavior.

## 5. Results and Discussion

The results and discussion are organized into two sections: Section 1 discusses the validation where comparison of results with the experiments of Morgenstern [2] is evaluated. Section 2 is dedicated to the cavity results with the effects of Reynolds number, aspect ratio (L/D) and thermochemical non-equilibrium flows.

### 1. Validation results

Before analysing the cavity flow physics, the computational set up was validated against the hypersonic cavity flow experiments of Morgenstern and Chokani (1994) [2]. The shape and configuration of the cavity is two dimensional rectangular hollow embedded in a flat plate subjected to hypersonic flow is used in the study. The cavity is open, with a shear layer flowing from the leading to trailing edges. The cavity aspect ratio (L/D) is critical in determining whether the cavity flow would be open, transitional, or closed. A Mach 6.3, two-dimensional hypersonic flow over a cavity was computed and validated against the experiments of Morgenstern and Chokani [2]. The tests were conducted at a total temperature of 1100 K, wall temperature fixed at 300 K, and Reynolds numbers per meter is $2.116 \times 10^6$ at Mach 6.3. The cavity aspect ratio (L/D) used in the validation is 10.67. The computational grid for the aspect ratio (L/D) is shown in Figure 1. The length of the upstream section (before cavity), cavity and downstream section (after cavity) are -315.6 mm, 203.8 mm and 280.2 mm. The structured grids are employed in this study.

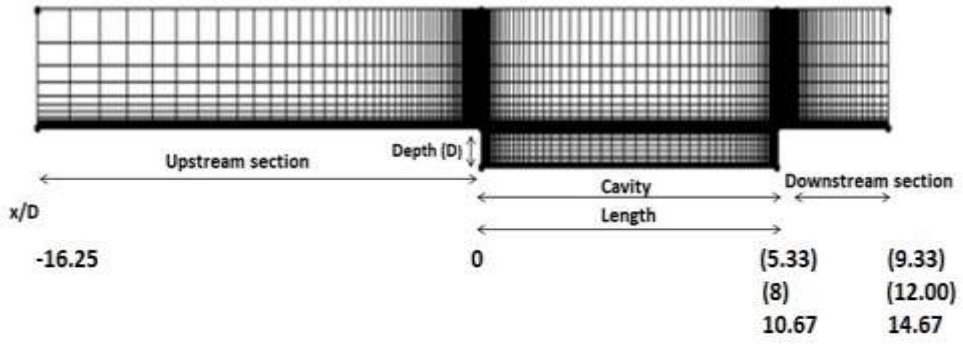


**Figure 1 Computational grid for the 10.67 aspect ratio cavity**

The comparison of the incoming velocity profile with experimental results, at an x/D station of -1.33 is presented in Figure 2. The plot shows how velocity varies with vertical position within a flow domain a boundary layer over a flat surface. There is a good agreement between the experimental and computed results with slight deviation. Near the wall both profiles start from nearly zero, satisfying the no-slip condition. Far from the wall, the velocity reaches freestream value (1.0), indicating that the boundary layer thickness is well captured. The comparison between computed and experimental heat transfer shows a consistent trend low values inside the cavity, followed by a steep rise near x/D≈10 as the flow reattaches past the trailing edge is presented in Figure 3. The numerical results capture both the location and magnitude of the main heating peak well, although they show a small secondary bump around x/D≈8 that is less evident in the experimental data. This difference is likely due to numerical prediction of a minor impingement inside the cavity. After reattachment, both datasets show the expected rapid drop in heat transfer as the flow settles back into a smooth boundary layer. A comparison of Mach number profiles at three streamwise location: upstream of the cavity (x/D= -1.33) and within the cavity (x/D=2.67 and 8) is shown in the Figure 4. The simulation accurately captures the upstream boundary layer, shear layer development, and wake recovery showing close agreement with experimental data across all positions. At x/D = -1.33 (upstream), the flow shows a classic boundary layer profile. Mach number increases with height undisturbed freestream flow. At x/D = 2.67 (Inside cavity / shear layer region), the profile is more distorted due to separation and shear layer effects. It reflects complex interactions between cavity recirculation and high-speed outer flow. At x/D =8 (rear of the cavity), Mach number profile is steep near the wall and smoothly transitions to freestream.

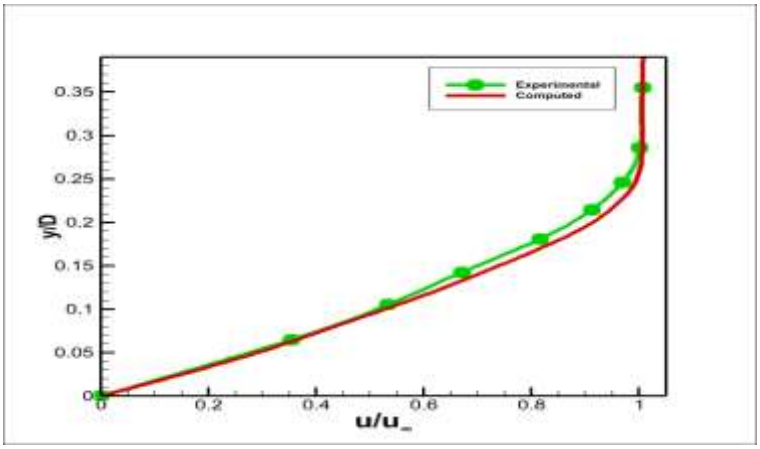


**Figure 2 Velocity profile at x/D= -1.33**

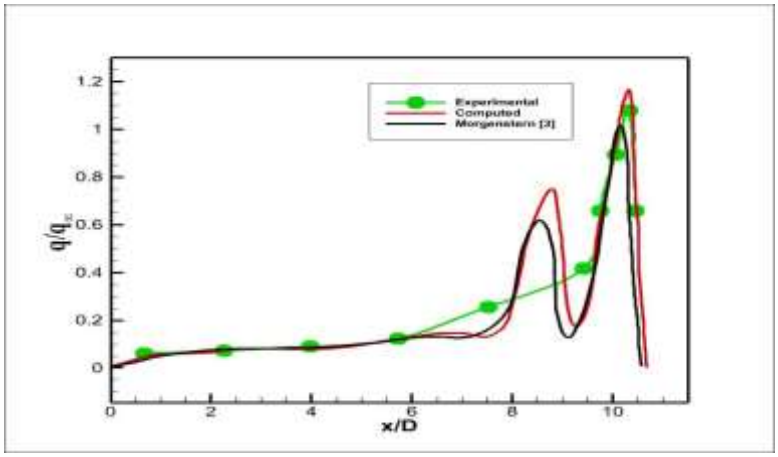


**Figure 3 Surface heat transfer ratio of the cavity**

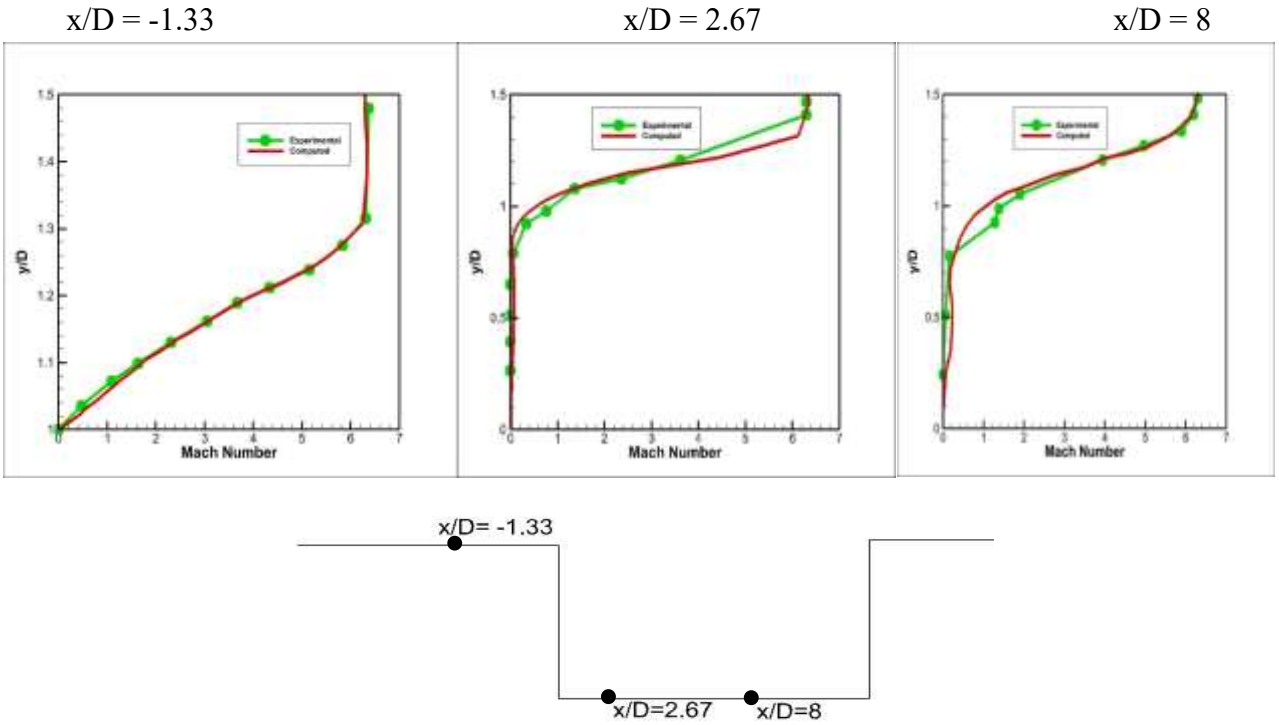


**Figure 4 Mach number profiles at x/D= -1.33, 2.67 and 8.**

## 2. Cavity results

In this section, the effect of aspect ratio, Reynolds number and thermochemical non-equilibrium is analysed and reported. The aspect ratios (L/D) were 5.33, 8.0 and 10.67. The cavity depth was kept constant and the cavity length was varied. The tests were conducted at a wall temperature fixed at 300 K and Reynolds numbers per meter are $1.033 \times 10^6$ to $4.085 \times 10^6$ [3]. Numerical calculations are performed at Mach number of 6.3.

In the present simulation structured grids are employed. Computational grids to solve numerically the different aspect ratios were chosen after the evaluation of grid independence analysis. Figure 5 shows the grid independence analysis based on comparing the velocity profile at an x/D station of -1.33. The details

of low, medium and high mesh resolutions are provided in the Table 1. Across all cases, the velocity begins at zero at the wall and gradually rises towards the freestream value as y/D increases, which aligns with the expected behaviour of a developing shear layer above the cavity with the experimental results. With the low mesh refinement, the velocity profile underestimates the outer flow, compared to experimental data suggesting that this grid is too coarse to capture the full shear layer growth and velocity gradients. Refining the mesh to fine delivers the best performance, providing a smooth and physically accurate transition from the near-wall region to the freestream, and closely aligning with experimental observations both in the steep near-wall gradient and in the gradual flattening in the outer region. These results clearly demonstrate that grid refinement enhances the resolution of the shear layer and improves agreement with experimental data. The consistency of the 1,02,000 cell mesh results with both the 90,100 cell case and experimental measurements indicates that mesh independence has been effectively achieved, ensuring that subsequent simulations are free from significant grid-induced errors. The grid independence analysis of surface heat transfer for L/D=10.67 is shown in the Figure 6. It tracks how surface heat flux varies along the length of the cavity and downstream surface. Inside the cavity, recirculating flow has low wall heat transfer due to low velocity gradients. Shear layer reattachment causes sudden spike in both wall shear stress and temperature gradient resulting in high heat flux at the reattachment point. Downstream of reattachment, the heat flux drops as the boundary layer thickens and gradients reduce.

These findings highlight that increasing grid resolution improves the ability to resolve shear layer features and enhances numerical stability. Given the convergence observed, the high refinement mesh was chosen for subsequent simulations involving variations in Reynolds number and cavity geometry.

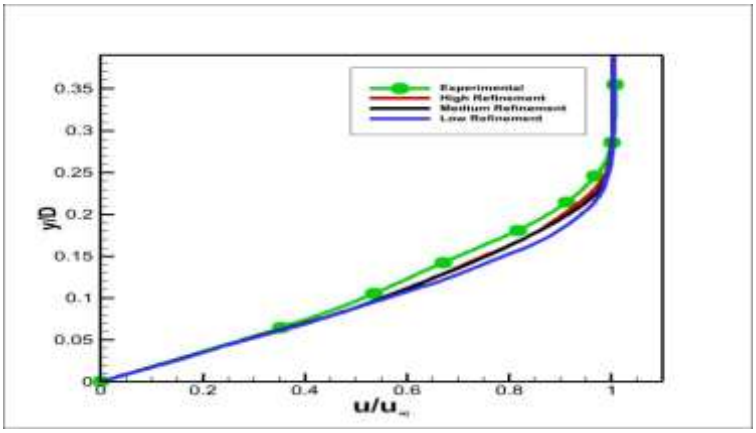


**Figure 5 Grid independence analysis for the L/D= 10.67, Mach 6.3**

**Table.1 Grid resolution used for the grid independence analysis**

| Grid | Total cells |
|---|---|
| Low Refinement | 80000 |
| Medium Refinement | 90200 |
| High Refinement | 102000 |

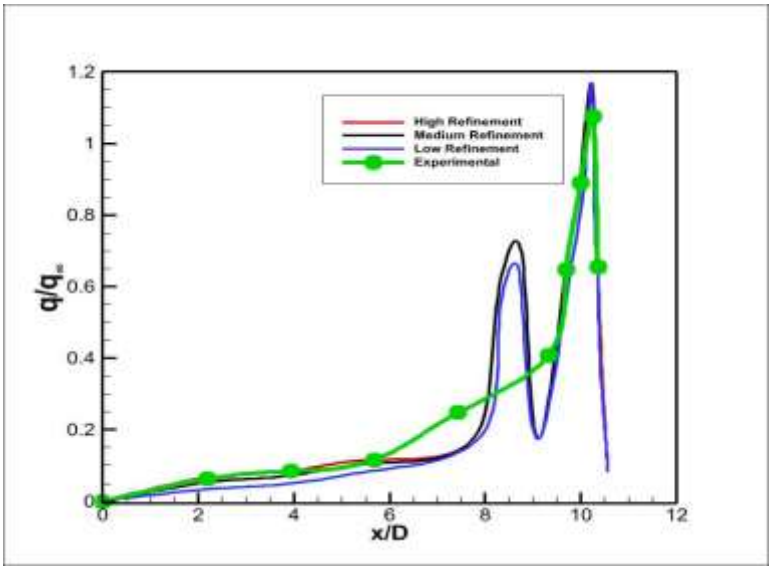


**Figure 6 Grid independence analysis on surface heat transfer ratio for L/D=10.67**

### 2.1 Effect of aspect ratio of the cavity at a fixed Reynolds number

The effect of an aspect ratio of the cavity at a fixed Reynolds number per meter is $2.116\times10^6$ is investigated keeping other conditions same. The temperature contours for the cavity aspect ratio of three is shown in the Figure 7. In all cases, the freestream flow skims over the cavity, forming a shear layer from the front to the back. Inside, a main swirling vortex dominates, with a smaller secondary vortex forming near the rear corner. For the smaller aspect ratio, the shear layer hits the rear wall more directly, creating a stronger, more compact main vortex and an energetic secondary vortex. In the larger aspect ratio, the flow has more space to develop, leading to a stretched main vortex and a weaker secondary one, with smoother, layered motion inside the cavity.

Figure 8 illustrates how normalized heat flux ($q/q_\infty$) varies along the downstream, cavity and upstream of the cavity (x/D) for aspect ratios L/D=5.33, L/D=8 and L/D=10.67. In all cases, the heat flux starts low near the leading edge and rises sharply where the shear layer strikes the floor. In figure 8(b) as L/D increases, this peak shifts downstream because the shear layer travels farther before impingement. The L/D=5.33 case shows a single strong peak, L/D=8 displays two distinct peaks, and L/D=10.67 exhibits multiple smaller peaks, reflecting more complex flow interactions. Overall, longer cavities tend to spread out the heating and delay the point of maximum heat flux. Figure 8(c) shows the normalized surface heat flux ($q/q_\infty$) downstream of a rectangular cavity in hypersonic flow for three cavity length-to-depth ratios (L/D). For all cases, heat transfer remains low inside the cavity due to flow separation, and then rises sharply at the reattachment point just after the trailing edge, where a strong shock–boundary layer interaction produces peak heating.

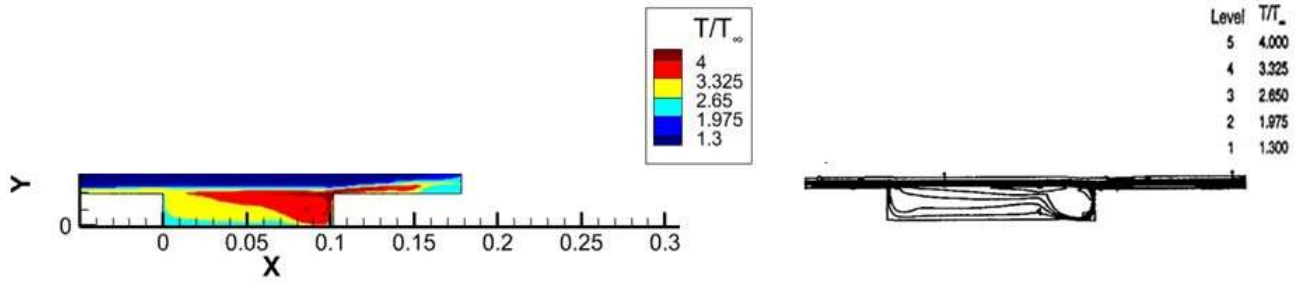


(a) L/D=5.33 Morgenstern paper [3]

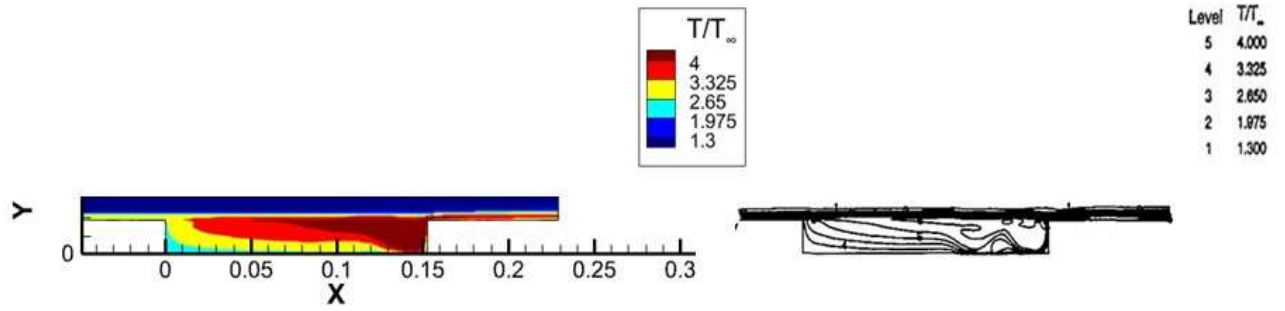


(b) L/D=8 Morgenstern paper [3]

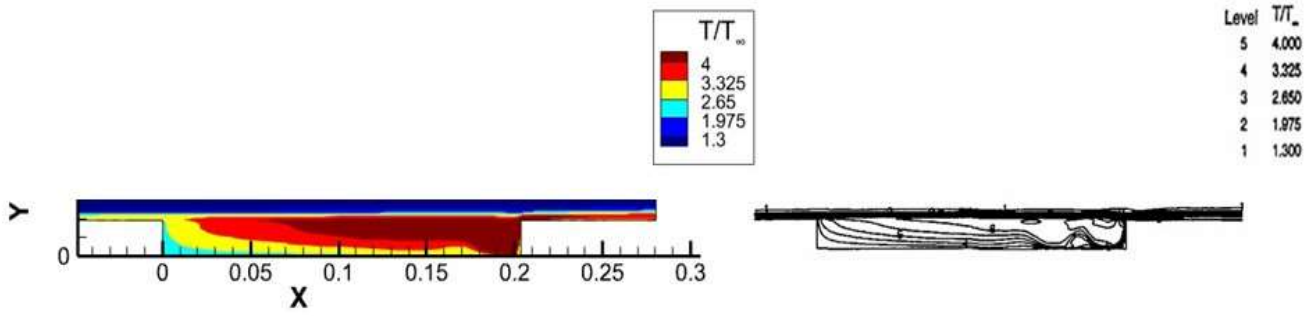


(c) L/D=10.67 Morgenstern paper [3]

**Figure 7 Temperature contours of (a) L/D= 5.33, (b) L/D= 8 and L/D =10.67**

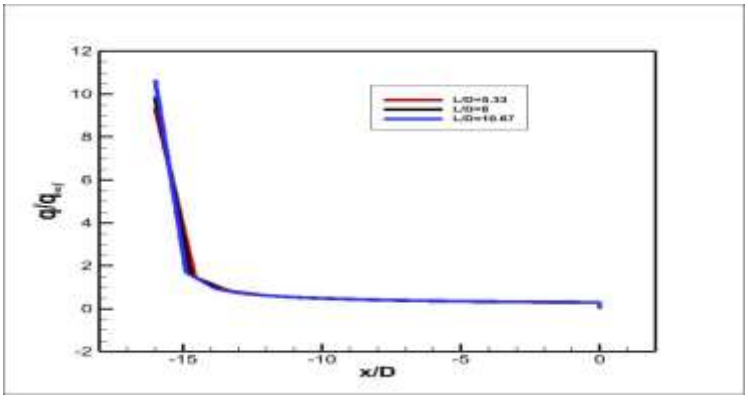


**(a) Upstream of the cavity**

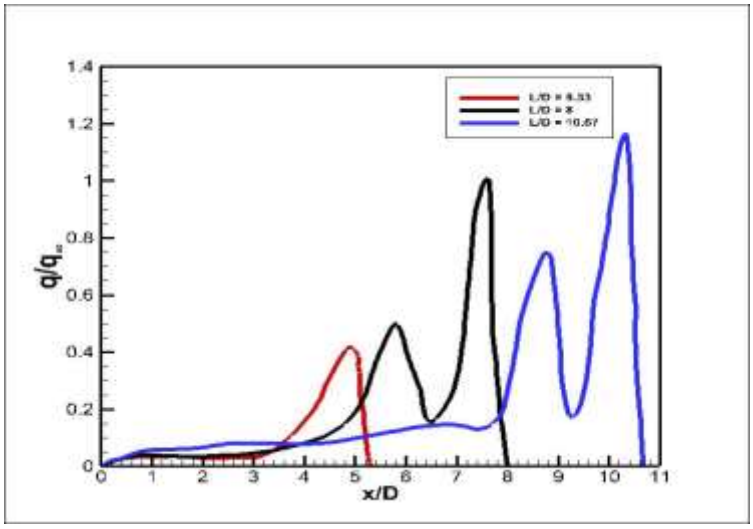


**(b) Cavity**

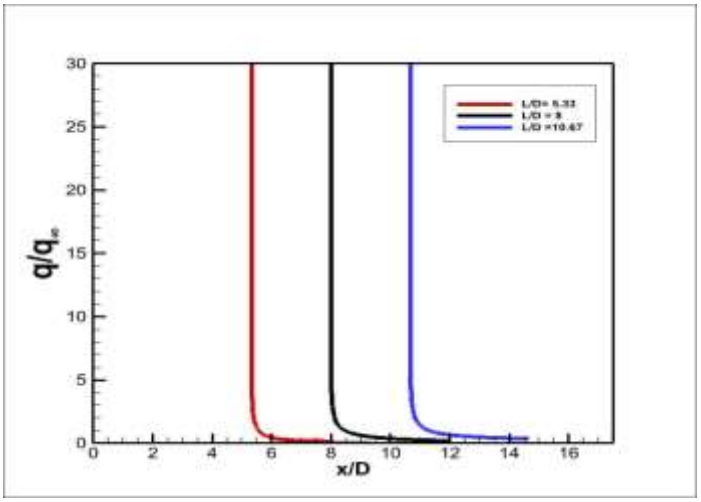


(c) Downstream of the cavity

**Figure 8 Surface heat transfer ratio for different cavity aspect ratios, Re/m=2.116x10$^6$**

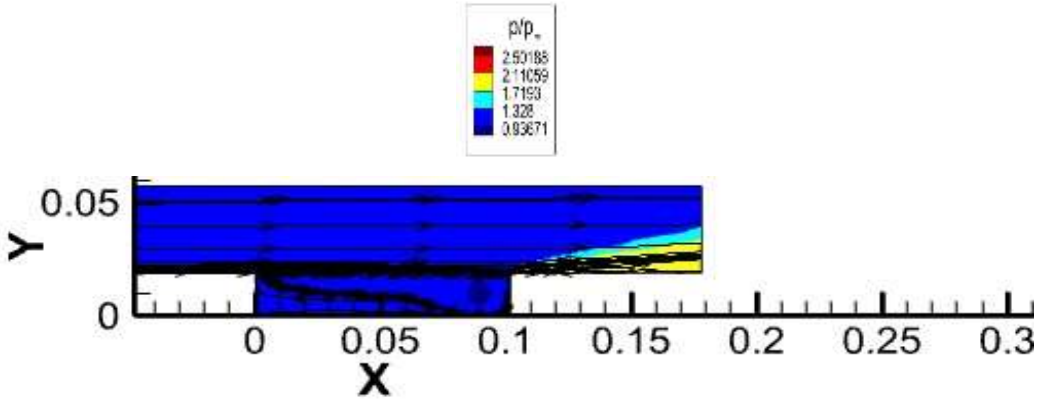


**(a)**

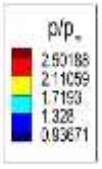

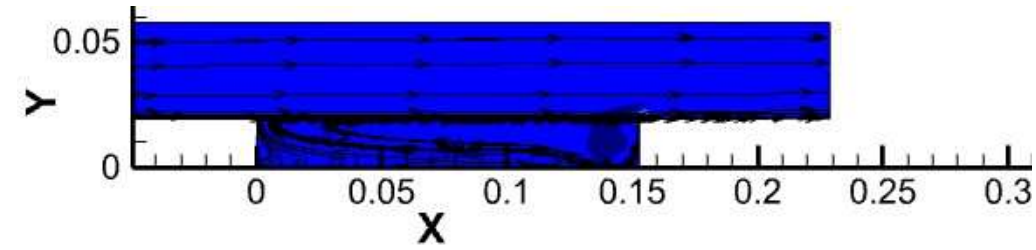


**(b)**

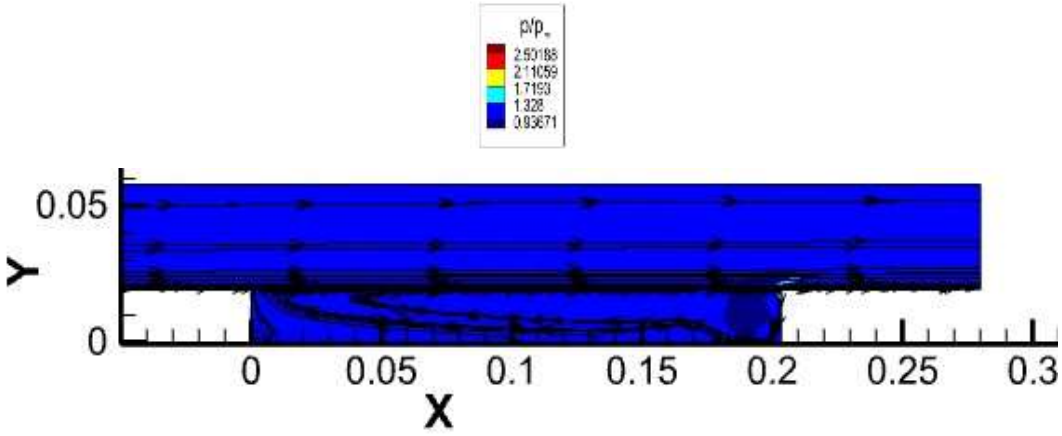


**(c)**

**Figure 9 Pressure contours for (a) L/D=5.33, (b) L/D=8 and L/D=10.67**

The pressure contours for the three aspect ratios are shown in the Figure 9. For the smallest L/D =5.33, the cavity is relatively short compared to its depth. The streamlines indicate a prominent, compact recirculation vortex near the downstream cavity wall, with the high-pressure region remaining limited to the downstream end. For L/D=8, the recirculation region elongates along the cavity floor, with streamlines showing more extended separation and a slightly broader high-pressure area near the cavity rear. The pressure distribution is less steep than in the shorter cavity, with more gradual changes from upstream to downstream wall. For the largest L/D =10.67, the cavity is longest relative to its depth. The vortex inside the cavity becomes even larger and stretches deeper into the cavity volume, interrupting the main flow over a wider span. In summary, as the L/D ratio increases, the internal flow structure transitions from a compact, intense vortex with steep pressure gradients and strong reattachment, to a broader, slower recirculation zone with more distributed pressure fields, affecting both aerodynamic heating and surface loading.

**2.2 Effect of a Reynolds number at a fixed aspect ratio**

The effects of a laminar Reynolds numbers of $1.033 \times 10^6$, $2.116 \times 10^6$ and $4.085 \times 10^6$ were studied at a fixed aspect ratio(L/D=10.67). Figure 10 shows the normalized surface heat flux ($q/q_\infty$) distribution along the streamwise direction for a rectangular cavity with L/D=10.67 at three Reynolds numbers. Heat transfer is minimal within the cavity but rises sharply at two key points downstream: a smaller peak near x/D≈8.5 due to intermediate flow impingement, and a larger peak just after the trailing edge (x/D≈10.67) caused by strong reattachment and shock–boundary layer interaction. Increasing Reynolds number amplifies both peaks, with the highest Reynolds number ($4.085 \times 10^6$) showing the most intense heating, indicating stronger convective transport and thinner boundary layers in hypersonic conditions.

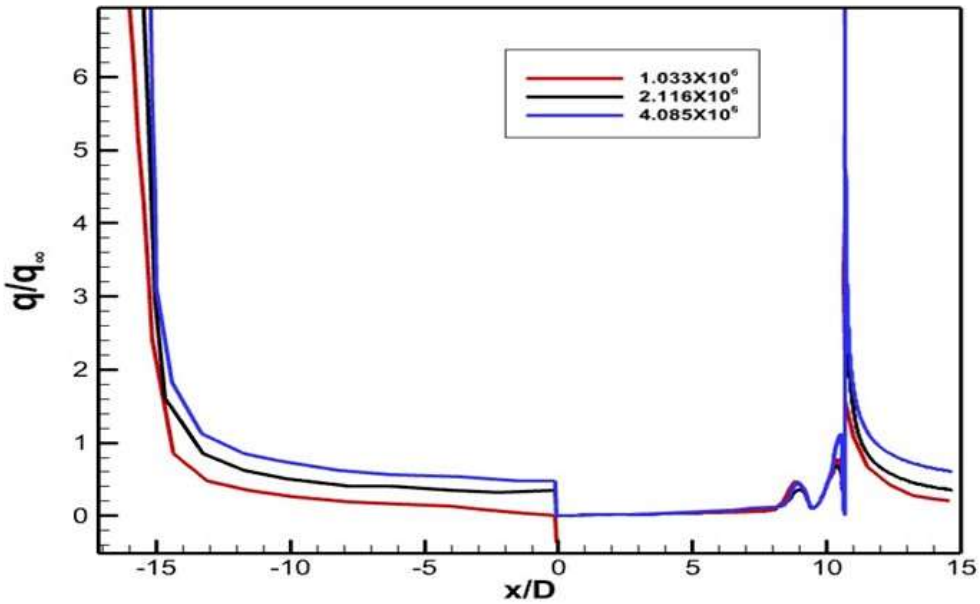


**Figure 10 Surface heat transfer ratio for different Re/m, L/D=10.67**

Right after the cavity's trailing edge, the heat transfer rises up sharply which a clear sign of the hot, high energy flow is reattaching to the surface. This spike is stronger at higher Reynolds numbers, with the highest case ($4.085\times10^6$) delivering the most intense heating. Moving further downstream, the heat transfer quickly drops off as the boundary layer settles back into a smoother, more stable flow. Strengthens, and secondary flow structures near the trailing edge become more distinct.

The velocity contour plots with streamlines show how changes flow inside and above a rectangular cavity with Reynolds number at a fixed aspect ratio is shown in Figure 11. At the lowest Reynolds number, the shear layer is thicker and the recirculating vortex inside the cavity is smaller, with less mixing. As Reynolds number increases, the shear layer thins, high-speed flow penetrates deeper, and the vortex grows stronger. At the highest Reynolds number, the flow is more energetic, with sharper velocity gradients and stronger interaction between the shear layer and the cavity walls.

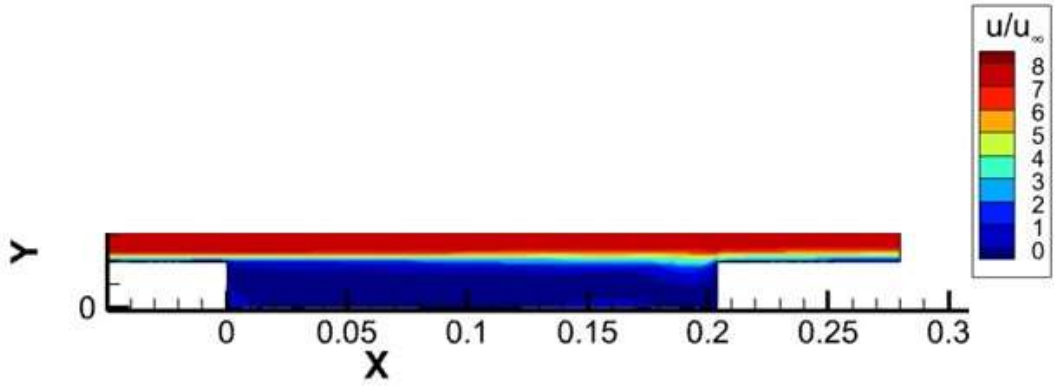


(a)

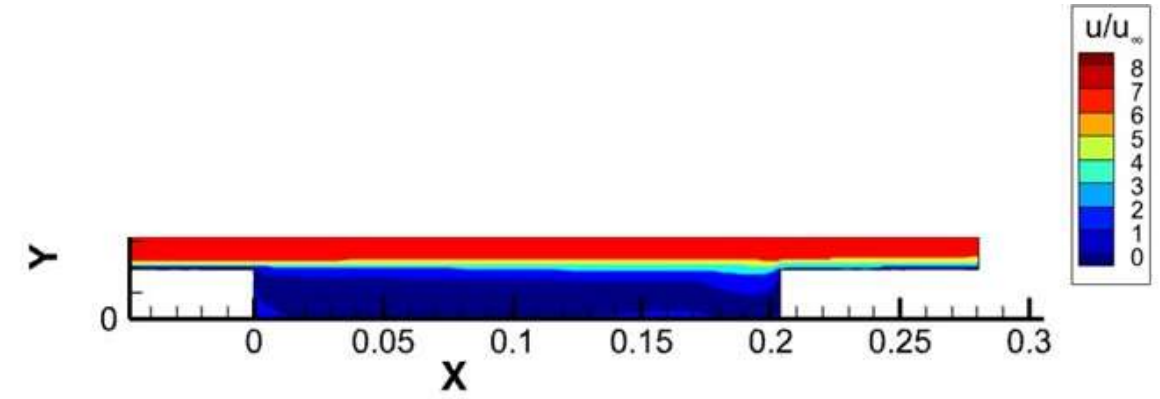


**(b)**

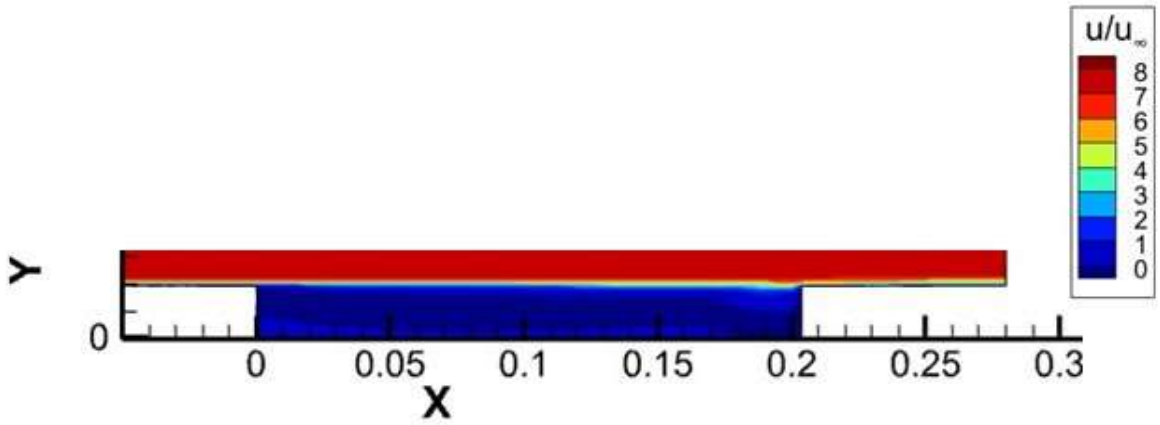


**(c)**

**Figure 11 Velocity contours of (a) $1.033\times10^6$, (b) $2.116\times10^6$ and (c) $4.085\times10^6$**

Figure 12 depicts the variation of the skin friction coefficient along a rectangular cavity subjected to hypersonic flow at varying Reynolds numbers. It highlights the typical flow separation within the cavity, evidenced by a negative skin friction region, followed by flow reattachment downstream. With increasing Reynolds number, the extent of the separation region decreases slightly and the reattachment point shifts accordingly, demonstrating the significant role of viscous effects on the cavity flow dynamics. Such insights are critical for accurate predictions of aerodynamic heating and drag in hypersonic applications involving cavity geometries.

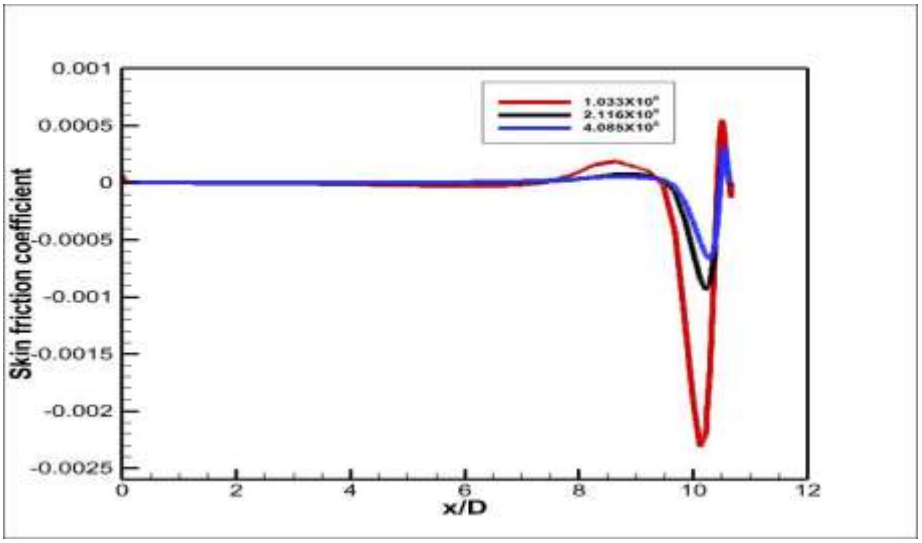


**Figure 12 Skin friction coefficient on surface of the cavity for different Reynolds number, L/D=10.67.**

### 2.3 Effect of Thermochemical non-equilibrium flow

Figure 13 compares the normalized surface heat flux ($q/q_\infty$) along the cavity floor for equilibrium flow and non-equilibrium flow under identical hypersonic flow conditions. The same flow conditions are used in this case. The non-equilibrium surface heat flux is consistently lower and exhibits smoother peaks compared to equilibrium predictions, especially near separation and reattachment regions on the cavity surface. Thermochemical non-equilibrium leads to less efficient energy transfer to the wall due to freezing of vibrational and chemical modes, meaning that not all internal energy released in shocks and boundary layers is immediately available to heat the surface. As a result, non-equilibrium flows tend to produce lower peak heating rates, more distributed gradients, and slightly delayed thermal responses compared to equilibrium flows under the same freestream and wall conditions.

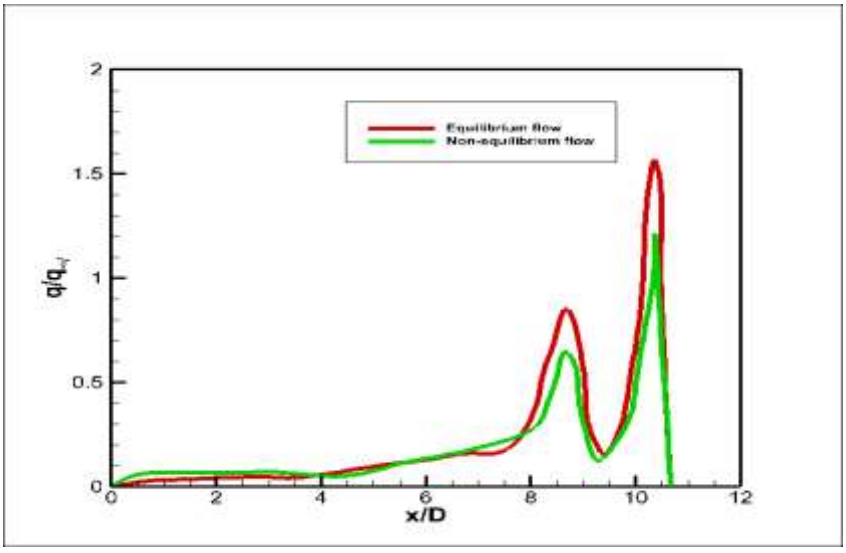


**Figure 13 Comparison of Equilibrium and non-equilibrium under identical flow conditions on surface heat transfer ratio.**

Figure 13 correctly illustrates that, for the same hypersonic flow parameters, non-equilibrium modelling gives more realistic (lower and less abrupt) surface heating trends due to incomplete energy relaxation and

slower chemical transformations behind shocks and inside recirculation zones. Hence there is a need to change the flow conditions. The freestream temperature, pressure are 1100 K and 7005 Pa and wall temperature at 1800 K.

Figure 14 shows the surface heat flux distribution normalized by the free-stream heat flux as a function of the position normalized by the cavity length (x/D) for two flow conditions: non-equilibrium and equilibrium. In hypersonic flows over cavities under different flow conditions, the heat flux distribution along the surface is strongly influenced by the flow state, showing relatively low heat flux upstream and sharply increasing near the cavity's trailing edge due to flow reattachment and shock interactions. Under non-equilibrium conditions, where vibrational and chemical relaxations are delayed, these heat flux peaks become significantly higher compared to equilibrium flow. Figure 15 illustrates how the skin friction coefficient changes along the surface for equilibrium and non-equilibrium hypersonic flow conditions over a cavity. The values remain close to zero upstream, but as the flow approaches and exits the cavity (near x/D=10), there are sharp drops followed by rapid increases, indicating regions where the flow separates and then reattaches. The non-equilibrium flow displays slightly lower minimum and different peak values compared to equilibrium flow, highlighting how delayed energy processes affect wall shear stresses.

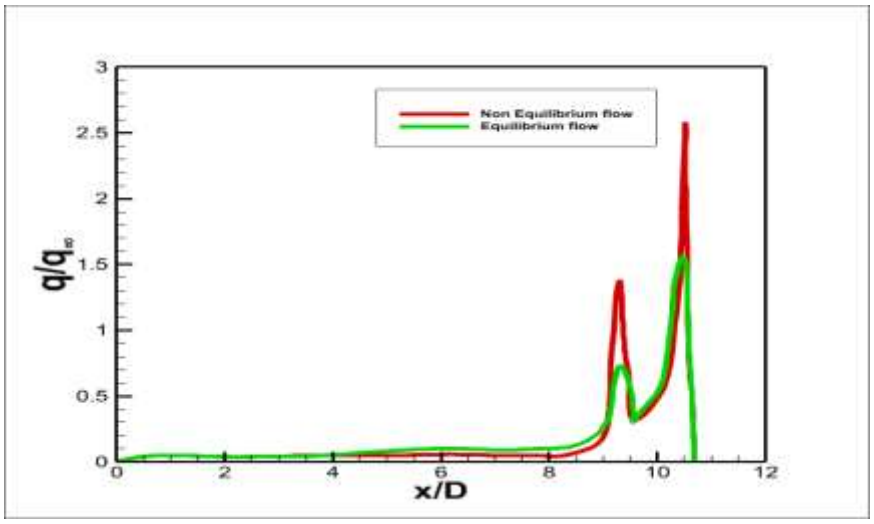


**Figure 14 Comparison of equilibrium and non-equilibrium under different flow conditions on Surface heat transfer ratio.**

Figure 16 illustrates the temperature distributions inside and around a rectangular cavity for hypersonic flow, highlighting transrotational temperature (Ttr) on the left and vibrational-electronic temperature (Tve). In the Ttr plot, increased temperatures are primarily confined to the near-wall region and especially pronounced at the cavity's trailing edge, indicating localized heating due to shock impingement and flow reattachment. By contrast, the Tve plot reveals that vibrational-electronic temperature builds up more significantly along the cavity floor and remains much higher deeper into the cavity, with more pronounced and widespread heating.

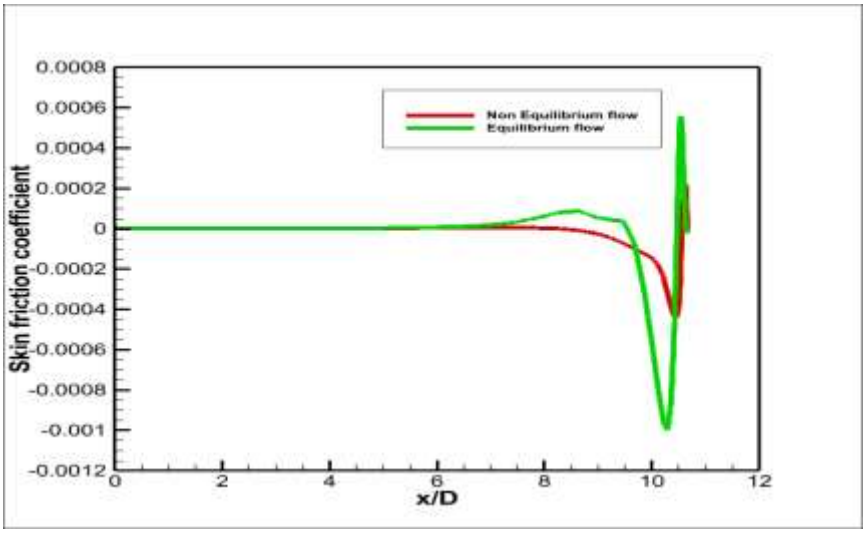


**Figure 15 Comparison of equilibrium and non-equilibrium under different flow conditions on skin friction coefficient.**

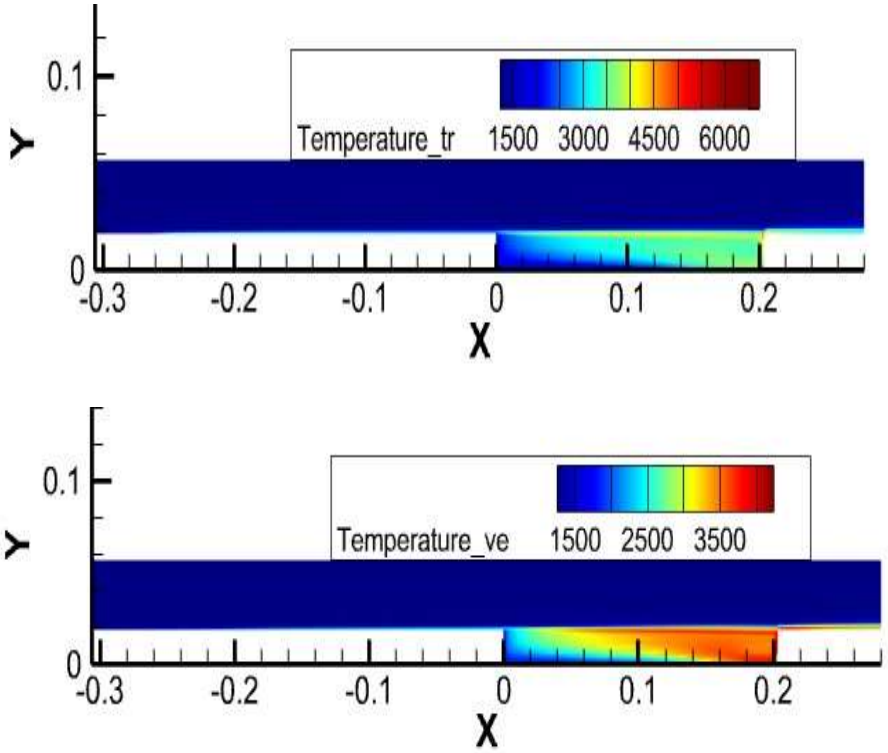


**Figure 16 Transrotational Temperature and Vibrational-electronic Temperature.**

## 6. Conclusions

A computational investigation of the hypersonic flow over a rectangular cavity has been accomplished. The study reveals that both cavity aspect ratio and Reynolds number substantially influence the flow physics inside and around rectangular cavities in hypersonic regimes. Reducing the aspect ratio intensifies shear layer–trailing wall interactions, producing stronger recirculation zones, higher localized pressure peaks, and increased thermal loads. In contrast, larger aspect ratios promote a more stable shear layer development, leading to a more uniform low-pressure core and reduced peak aerodynamic and thermal loads.

The effect of Reynolds number on the hypersonic flow over a rectangular cavity creates a strong shear

layer that spans from the leading to the trailing edge, trapping a large recirculating vortex inside. This flow pattern produces low heat transfer within the cavity but generates intense heating just after the trailing edge, where the flow reattaches and interacts with the wall through a strong shock. Higher Reynolds numbers amplify this effect, leading to stronger vortices, sharper reattachment shocks, higher local pressures, and significantly increased peak heat flux. Beyond this reattachment point, the flow stabilizes, and both pressure and heat transfer rapidly decline as the boundary layer redevelops. These combined effects underscore the critical role of geometric scaling and flow conditions in cavity flow control, with direct implications for aerodynamic performance, structural loading, and thermal protection system design in high-speed vehicles.

**References**

1. Hahn, M., (1969) "*Experimental Investigation of Separated Flow over a Cavity at Hypersonic Speed*," *AIAA Journal*, Vol. 7, No. 6, 1969, pp. 1092-1098.
2. Donald E. Nestler, (1982) "*An experimental study of hypersonic cavity flow*," *Journal of Spacecraft*, VOL. 19, NO. 3, MAY-JUNE 1982.
3. Algacyr Morgenstern Jr. and Ndaona Chokani, (1994) "*Hypersonic Flow Past Open Cavities*," *AIAA Journal*, Vol. 32, No. 12, December 1994.
4. A. P. Jackson, R. Hillier and S. Soltaniy, (2001) "*Experimental and computational study of laminar cavity flows at hypersonic speeds*," *J. Fluid Mech.*, vol. 427, pp. 329-358.
5. Joel L. Everhart, Stephen J. Alter, N. Ronald Merski, William and Ramadas K. Prabhu, (2006) "*Pressure Gradient Effects on Hypersonic Cavity Flow Heating Sciences*," AIAA Conference Paper 2006-0185.
6. E.M. Wahba, "*On the steady flow in a rectangular cavity at large Reynolds numbers: A numerical and analytical study*," *European Journal of Mechanics B/Fluids* 44 (2014) 69–81. doi: 10.1016/j.euromechflu.2013.10.005
7. Thomas J. Scanlon, James Weir and Jason M. Reese, (2012) "*Aerothermodynamic Comparison of Two and Three-dimensional Rarefied Hypersonic Cavity Flows*," *Journal of Spacecraft and Rockets*, Vol. 51, No. 5, 2012.
8. S K Singh, J Chowdhury, S Ghosh, P K Raushan, K Debnath & P Kumar, (2019) "*Experimental and numerical investigation of flow characteristics in an open rectangular cavity*," *ISH Journal of Hydraulic Engineering*, 2019, DOI: 10.1080/09715010.2019.1665482
9. Jeremy Redding, Jacob Gamertsfelder, LuisBravo, and Prashant Khare, (2023) "*Thermochemical non-equilibrium hypersonic flow over a rectangular cavity embedded on a compression ramp*," *Physics of Fluids*, 35, 126101 (2023). DOI: 10.1063/5.0172435
10. D. Passiatore, L Sciacovelli, P Cinnella and G Pascazio, "*Thermochemical non-equilibrium effects in turbulent hypersonic boundary layers*," *J. Fluid Mech.* (2022). DOI: 10.1017/jfm.2022.283
11. Palacios, F., Alonso, J., Duraisamy, K., Colonno, M., Hicken, J., Aranake, A., Campos, A., Copeland, S., Economon, T., Lonkar, A., et al., (2013) "Stanford University Unstructured (SU2): An Open-Source Integrated Computational Environment for Multi-Physics Simulation and Design," 51st AIAA Aerospace Sciences Meeting Including the New Horizons Forum and Aerospace Exposition, AIAA Paper 2013-0287, 2013.